anticipated, dissimilar IR responses were observed per location and therefore reasonable to predict similar behaviors for the SNR^0_{Rcv} responses at those locations. This is corroborated subsequently.

4.1.2 Received SNR, SNR^0_{Rcv}, measurement: Following the immediately outlined channel IR measurements, the measured SNR^0_{Rcv} responses distributed over the passenger plane grid was completed and shown in Fig. 7. A steady background noise (includes

Fig. 7: Measured $SNR^0_{Rcv}(x, y)$ in-car.

noise floor) of -91 dBm was observed in-car and rapid fluctuations apparent in the passenger plane (Fig. 7). This is in line with the dissimilar IRs of Section 4.1.1, is due to the rich multipath behavior inside the car body and is corroborated by the multiple echoes of the direct path with fading (path-loss attenuation) observed in Fig. 6. The statistical properties of the measured SNR^0_{Rcv} data were: maximum 14.1 dB, minimum 8.1 dB, mean 11.1 dB, and standard deviation 0.16 dB. In addition, the highly fluctuated SNR^0_{Rcv} of Fig. 7 does not assure an equal target BER over the passenger plane grid and justifies the need of measuring the entire grid plan (N points); this is because the BER response will also fluctuate and differ from the η. Since the signal strength is dependent on the antenna efficiency, the SNR^0_{Rcv} can be improved and meet the target BER η by redefining the radiation pattern of the access point antenna, next.

4.2 Stage-2: The BER and the SF_d

In this section, the BER and the desired antenna space-factor (SF_d) performance in-car is evaluated. The adapted UWB MB-OFDM model presented in Section 3.2 is used and the UWB channel custom block redefined using a friendly graphical user interface (GUI) with setting parameters that considered the system behavior in the following communication channels, statistical AWGN, CM1 -4, and the channel measurements reported in Section 4.1. The evaluation process comprises two phases, 1) the predicted BER performance using the earlier experimentally measured in-car channel and 2) the SF_d for improved BER responses in-car.

4.2.1 The predicted BER vs. E_s/N_0 performance using the measured $h^0(t, x, y)$ and SNR^0_{Rcv}: Essentially, how the in-vehicle environment affected the channel model is shown in Fig. 8 where a deviation in the E_s/N_0 responses compared to other statistical models, CM1-4, was observed. The MB-OFDM performance was initially characterized in an AWGN channel to obtain the minimum SNR for target BER η and helped quantifying the effect of channel dispersion; the SNR was found to be ∼7.4 dB. Dissimilar SNR-BERs in each mobile equipment (ME) location encouraged measuring the multiple locations in-car and established the target SNR γ (where the BER crosses η) for 220 measured mobile equipment locations in-car; only 3 locations are shown for clarity. Results corroborate the predictions presented in Section 4.1.2, where dissimilar BER performances were anticipated in the passenger grid plan (N points). This justifies the use of the 220 readings (a high number means accuracy) and the practical on-site measurements overcome unrealistic statistical channels in this application - unrealistic because these canonical form channels do not fully describe the in-car application presented in this manuscript. The slightly improved performance on CM4 over the CM1 (LOS) was due to the car body acting as a reverberation channel which favored from the collection of multipaths.

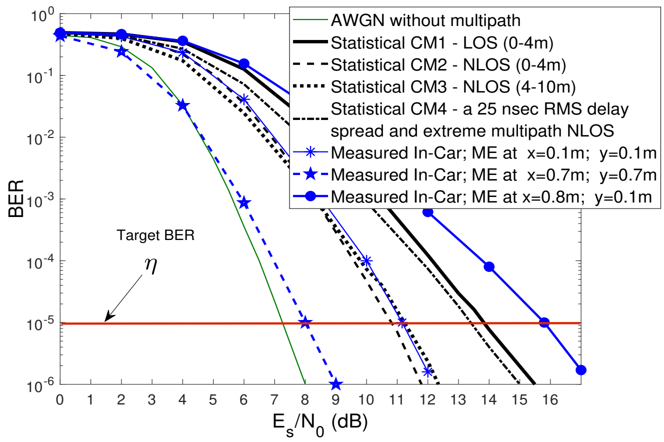

Fig. 8: BER vs. E_s/N_0 using statistical and measured channels with different IRs.

4.2.2 The $SF_d(x, y)$ that attains the target BER performance in the passenger plan (N points): For the assessment, $\gamma(x, y)$ is calculated using (4) and $\gamma = E_s/N_0 \times (f_s/B)$, where f_s is the channel data rate and B the bandwidth. The result is plotted in Fig. 9(a) and shows a $\gamma(x, y)$ as dictated by the $\eta = 10^{-5}$ (Fig. 8). A histogram, presented in Fig. 9(b), shows the highly varied γ responses over the passenger plane grid, corroborates the need of measuring N points, and prevails over the predominantly use of statistical channel models for their lack of accuracy (scarce number of registered data points [17–23]) in this application.

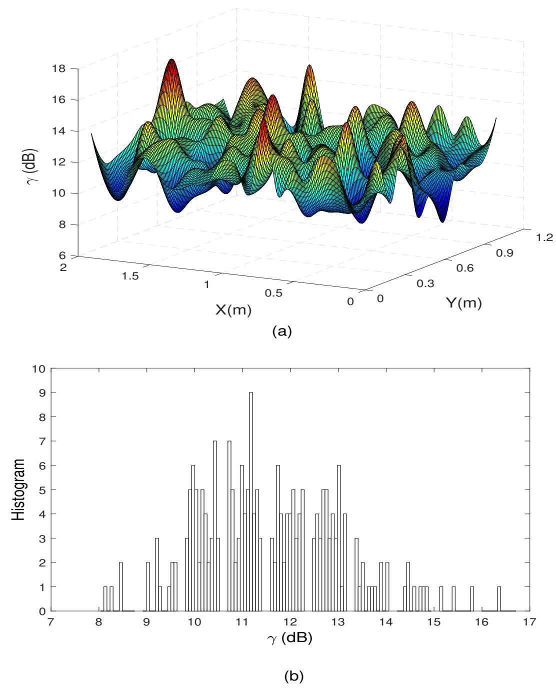

Fig. 9: (a) The calculated $\gamma(x, y)$ in-car, and (b) the histogram of the γ.

Following the calculated $\gamma(x,y)$, the $SF_d(x,y)$ was found. For the calculation, (8), evolving the SNR^0_{Rcv} (Fig. 7) and the γ (Fig. 9a), was used. The result is plotted in Fig. 10 and used to optimize the physical aperture of the prospective antenna and its associated continuous source distribution, next.

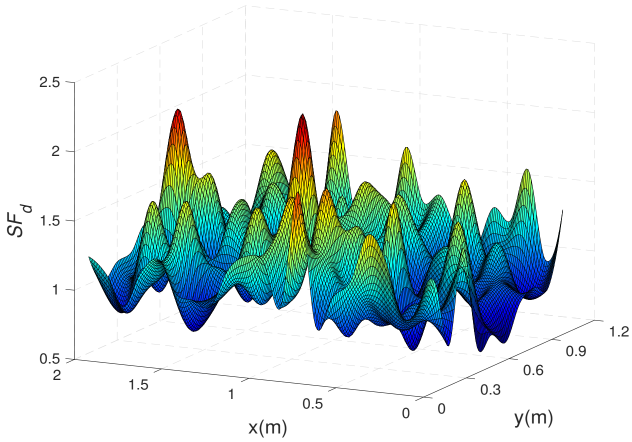

Fig. 10: The calculated desired antenna space-factor $SF_d(x,y)$ in-car.

4.3 *Stage-3: Radiation pattern-and-source synthesis*

The physical aperture and associated continuous source distribution of the prospective antenna is now determined. Particularly, the Woodward-Lawson pattern synthesis technique introduced in Section 3.3.2 and the SF_d response presented in Fig. 10, is used to determine the required continuous source, $I_{fin}(x',y')$ and $\Phi_{fin}(x',y')$. The SF_d was obtained using 220 N points since a higher number of samples in (20) yields to a highly complex inverse operation to matrix (16). Hence, we limited the number of samples to N_s, $\rightarrow N_s \leq N$. Due to the limitations of using N_s (rather than N), the BER adjusts to BER^{fin} and hence to SF_{fin}. Since N_s defines the physical aperture of the antenna, Fig. 4, whose dimensions $l_x = l_y = \lceil\sqrt{N_s}\rceil\lambda$, [37], the lower the N_s, the smaller the aperture (preferred). But, as N_s impacts on the BER performance (later corroborated in this Section), we established herein a prospective antenna design whose N_s is the optimization parameter to minimize the blind spots (1) in-car.

To find the continuous source (18) required by the antenna we rearranged the initial goal (2) such that the optimization problem becomes:

$$\begin{aligned} &\underset{N_s}{\text{Minimize}} && \%\text{Blind Area}\,(1) \\ &\text{subject to} && N_s \leq N, \end{aligned} \tag{22}$$

To determine the appropriate N_s value, we close looked at the individual $N = 220$ samples of the SNR^0_{Rcv} (Fig. 7) and selected those samples with deprived SNR; the selected samples correspond to those deeply faded responses in the passenger grid plan. To improve the received signals in-car and the BER consequently, we computed the minimum blind-area solution probable and the continuous source coefficients for that solution, next.

4.3.1 *The optimization of the blind-areas in-car:*

We used (22) and the Woodward-Lawson synthesis of Section 3.3.2 for the purpose and plot aided by Matlab the percentage blind-area in regards to N_s in Fig. 11. The response is non-monotonic with N_s settled to the adopted scheme and not to a synthesized antenna size. By observation, the overall blind-area is N_s dependent and severely varies upon N_s. Furthermore, values of $N_s > 17$ have no real solution since the inverse matrix calculation of the invertible square matrix (16) is singular (not feasible) to working precision. Therefore

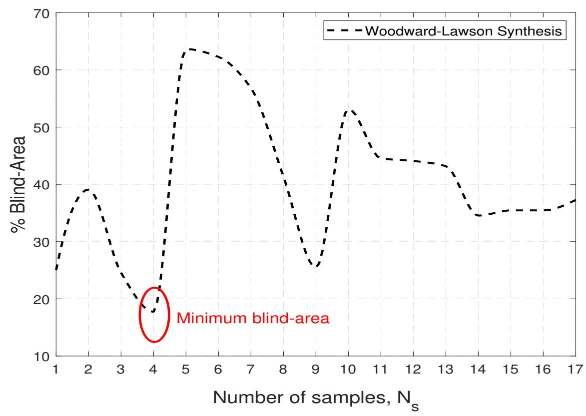

Fig. 11: The minimum blind-area in-car used for optimization.

N_s is limited to $1 \leq N_s \leq 17$ and the optimized solution to (22) found to be $N_s = 4$ (the lowest blind-area in Fig. 11). This is in fact the 4 lowest SNRs in the passenger grid plan and will be demonstrated, later in Section 5, to be an optimal value for the improved BER performances in-car.

4.3.2 *The required continuous source coefficients:*

We used the immediately reported $N_s = 4$, which in fact corresponds to 4 optimal samples of the SF_d (Fig. 10). Since the continuous source coefficients (amplitude and phases) can be found from the SF_d (by finding $[b_n]$), Section 3.3.2, hence, we use the inverse pattern synthesis technique to retrieve every $I_{fin}(x',y')$ and $\Phi_{fin}(x',y')$ composing the prospective antenna's physical aperture. The result is depicted in Fig. 12, and leads to an antenna (Fig. 4) of dimensions $l_x = l_y = \lceil\sqrt{N_s}\rceil\lambda = 2\lambda$. Using the antenna's physical aperture as

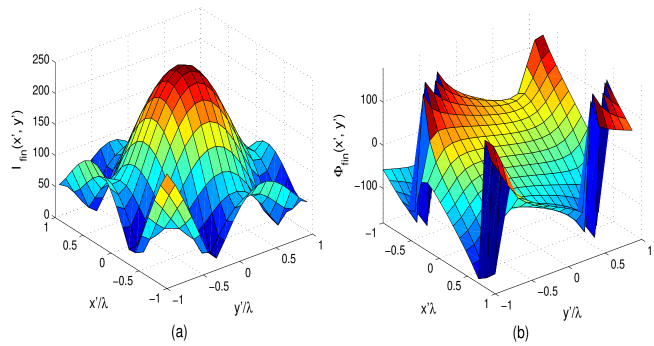

Fig. 12: Required continuous source coefficients (a) $I_{fin}(x',y')$ (b) $\Phi_{fin}(x',y')$ showing the prospective antenna's physical aperture in regards to wavelength, λ.

a contribution of the continuous source coefficients immediately outlined (shown in Fig. 12), the $SF_{fin}(x,y)$ of the prospective antenna is calculated and the result depicted in Fig. 13. Primarily given by the computational limitations of $N_s \leq N$ and the inherent antenna's aperture dimensions, the SF_{fin} differed from the SF_d, but did not present inhibition for improving the UWB MB-OFDM communications in-car. This is corroborated in the results section, subsequently.

5 Results

The improved in-vehicle UWB MB-OFDM communications is evidenced from the improved responses (BER and blind-area) obtained when using the prospective antenna compared to the standard and is detailed next.

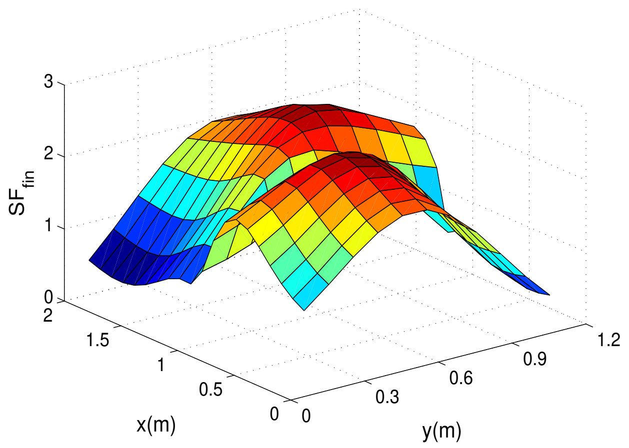

Fig. 13: The calculated $SF_{fin}(x, y)$ in-car using the prospective antenna as access point.

5.1 *The improved BER*

Using the adapted Simulink model presented in Section 3, the BER performance in-car is predicted when using the standard antenna and the prospective antenna for the access point. Comparison results show the $BER^0(x, y)$ vs. the $BER^{fin}(x, y)$, in Fig. 14(a) and (b) respectively, distributed over the passenger grid plan in a color map surface plot form. By observation, the BER performance in-car is outperformed for the case where the prospective antenna is used since a far inferior number of blind-areas ($BER > 10^{-5}$) are apparent. The blind areas still present in Fig. 14(b) depended on the selection of the N_s samples that were used for optimization. This value was limited upon the antenna realization (realistic size) to 4 (Section 4.3) and led to few error rates in certain points of the grid plan. Yet, a largely improved error rate is seen as a whole. The accomplished $BER^{fin}(x, y)$ is therefore principally achieved as a result of the well-defined continuous source coefficients, $I_{fin}(x', y')$ and $\Phi_{fin}(x', y')$) of Fig. 12.

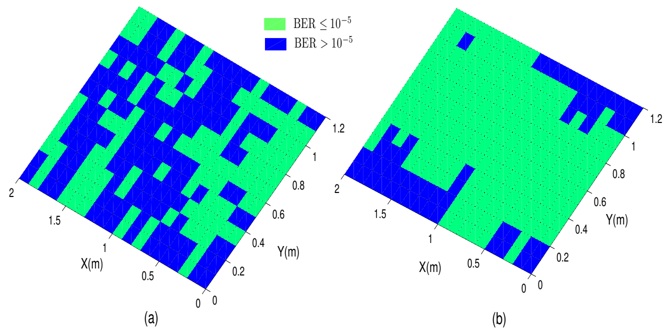

Fig. 14: The predicted BER in-car (a) BER^0 using the standard antenna (b) BER^{fin} using the prospective antenna

5.2 *The improved blind-area*

Using the results of Fig. 14, the percentage blind-area was computed for comparison between the responses of the prospective antenna vs. those of the standard when used as access point. The comparison is provided in Table 1 and the result achieved by the prospective antenna reduced the %Blind-Area (1) in 37.73% compared to that of the standard antenna. This translates into high-efficient (capacity and data rate) UWB-OFDM communications in-car.

Table 1 Performance comparison when using the prospective antenna vs. the standard antenna for the access point.

	% Blind Area
Standard Antenna	55.45%
prospective Antenna	17.72%

5.3 *Feasible antenna solution*

The prospective antenna gained from this research contribution is given by continuous source coefficients (amplitudes and phases) composing the antenna's physical aperture. The fabrication of this feasible antenna is suggested as future research. Although the rectangular-like planar aperture of the antenna ($l_x = l_y = 2\lambda$) was found tolerable for the in-car application, to exactly reflect the $I_{fin}(x', y')$ and $\Phi_{fin}(x', y')$ on a continuous antenna aperture (i.e: a patch) needs to be addressed, but seems to be a better solution than an array-made antenna since the feeding network of the array would be large and lossy. The antenna-array becomes large since multiple source coefficients would be required to form the array elements. A discretization of the continuous source (e.g., discrete source) can be used to estimate the radiation pattern of the antenna close to the SF_d [37]. The accuracy of this radiation pattern depends on the sampling occurrence, the permissible difference between the SF_d and the approximate pattern, and the BER_{fin}. The sampling can be met using the Root-Matching and perturbation techniques [40]; all have their own limitations over accuracy. Prototypes based on dielectric-made domes for shaping the antenna's radiation pattern [41] are suggested for investigation using the hereby proposed channel-based antenna synthesis; that would bring antennas with spatially selective gains, ideal for the antenna solution.

6 Conclusion

A channel-based antenna synthesis for improved in-vehicle UWB MB-OFDM communications has been proposed and presented. The synthesis allows for optimizing an antenna design for the scenario. The radiation pattern (an optimized SF) of the antenna (given by continuous source coefficients and a rectangular-like planar aperture) was modeled to provide improved in-vehicle UWB communications. This was achieved by an antenna whose SF provided (uniform) SNR-BER response in the passenger plane in-car and attributed to lowering the blind spots in the plane. Although this synthesis can be applicable to other vehicles, the extrapolation of the contemporary SF is limited to cars of similar dimensions since the IRs of the channel would vary. Any variation in the channel might not significantly influence on the primary antenna selection, but if a fully customized antenna is desired a new set of measurements should be performed. To corroborate the improved BER performance in-car, the results obtained using the prospective antenna were compared to those of a standard antenna. A new set of in-car channel measurements was performed, using the standard antenna, to overcome the unrealistic behavior of existing channel models in this scenario. The BERs were predicted using this genuine channel and provided the basis for estimating the SF of the access point antenna. The use of the prospective antenna showed an alleviated blind-area performance compared to that using the standard antenna and supports the optimized design (SF + continuous source coefficients + rectangular-like planar aperture) as a candidate for the access point in high-efficient UWB-OFDM communications in-car.

7 References

1 I. J. Garcia Zuazola, J. M. H. Elmirghani, and J. C. Batchelor, "High-speed ultra-wide band in-car wireless channel measurements," *IET Communications*, vol. 3, no. 7, pp. 1115 – 1123, July 2009.

2 I. J. G. Zuazola, L. Azpilicueta, A. Sharma, H. Landaluce, F. Falcone, I. Angulo, A. Perallos, W. G. Whittow, J. M. H. Elmirghani, and J. C. Batchelor, "Band-pass filter-like antenna validation in an ultra-wideband in-car wireless channel," *IET Communications*, vol. 9, no. 4, pp. 532 – 540, March 2015.

3 "First report and order, revision of part 15 of the commissions rules regarding ultra-wideband transmission systems," FDD, Tech. Rep. ET Docket 98-153, Feb.

2002.
4 S. Roy, J. Foerster, V. Somayazulu, and D. Leeper, "Ultrawideband radio design: the promise of high-speed, short-range wireless connectivity," *Proc. IEEE*, vol. 92, no. 2, pp. 295–311, Feb. 2004.
5 A. Batra and et al., "Multiband OFDM physical layer specification," WiMedia Alliance, Release 1.1, July 2005.
6 V. S. Somayazulu, J. R. Foerster, and S. Roy, "Design challenges for very high data rate UWB systems," in *Asilomar on Systems, Signals, and Computation*, Nov 2002, pp. 717 – 721.
7 IEEE 802.15 WPAN High Rate Alternative PHY Task Group 3a (TG3a). [Online]. Available: http://www.ieee802.org/15/pub/TG3a.html
8 A. Batra and et .al., "TI physical layer proposal for IEEE 802.15 task group 3a," IEEE P802.15-03/142r2-TG3a, March 2003.
9 ——, "Multi-band OFDM physical layer proposal," IEEE P802.15-03/268r0-TG3a, July 2003.
10 *ECMA-368*, Std., December 2008. [Online]. Available: http://www.ecma-international.org/publications/standards/Ecma-368.htm
11 S. H. Kratzet, "MB-OFDM and DS-UWB ultra-wideband design using SystemView by Elanixw," Eagleware-Elanix App Note AN-24B, March 2005.
12 G. Khuandaga, A. Iqbal, and K. S. Kwak, " Analysis of Modulation Schemes in Intra Vehicle Communications (IVC) Channel," in *13th International Conference on Advanced Communication Technology (ICACT)*, Feb. 2011, pp. 725–729.
13 X. Yin, J. Liu, Y. Su, X. Xiong, and G. Xiong, "A low-complexity synchronizer for OFDM-UWB-based vehicular communications," *IEEE Access*, vol. 5, pp. 7272–7284, 2017.
14 A. Batra, J. Balakrishnan, G. R. Aiello, J. R. Foerster, and A. Dabak, "Design of a Multiband OFDM System for Realistic UWB Channel Environments," *IEEE Transaction on Microwave theory and Techniqques*, vol. 52, no. 9, pp. 2123–2138, Sept. 2004.
15 J. Foerster, "Channel modeling sub-committee report final," *IEEE, P802.15-02/368r5-SG3a*, 2002.
16 A. Saleh and R. Valenzuela, "A statistical model for indoor multipath propagation," *IEEE Journal on selected areas in communication*, vol. 5, no. 2, pp. 128–137, Feb. 1987.
17 P. C. Richardson, W. Xiang, and W. Stark, "Modeling of Ultra-Wideband Channels Within Vehicles," *IEEE Journal on selected areas in communication*, vol. 24, no. 4, pp. 906–912, april 2006.
18 Y. Katayama, K. Terasaka, K. Higashikaturagi, I. Matunami, and A. Kajiwara, "Ultra-Wideband Impulse-Radio Propagation for In-Vehicle Wireless Link," in *64th IEEE Vehicular Technology Conference, VTC Fall*, Montreal, Quebec, Canada, 25-28 September 2006.
19 W. Niu, J. Li, and T. Talty, "Intra-vehicle UWB channels in moving and staionary scenarios," in *IEEE MILCOM*, Oct. 2009, pp. 1–6.
20 J. Mar, Y.-C. Yeh, and C.-C. Kuo, "Novel UWB In-Vehicle Channel Measurement Approach Based on Chirp Pulse Sounding Signal," in *International Symposium on Intelligent Signal Processing and Communication Systems (ISPACS 2009)*, Dec. 2009.
21 Y. Jin, D. Kwak, and K. S. Kwak, "Performance Analysis of Intra-vehicle Ultra-Wide Band Propagation in Multi-user Environments," in *IEEE 1st International Workshop on Vehicular Communications, Sensing, and Computing (VCSC)*, June 2012.
22 D. W. Matolak and A. Chandrasekaran, "5 ghz intra-vehicle channel characterization," in *IEEE Vehicular Technology Conference (VTC Fall)*, 2012, pp. 1–5.
23 C. U. Bas and S. C. Ergen, "Ultra-wideband Channel Model for Intra-vehicular Wireless Sensor Networks Beneath the Chassis: From Statistical Model to Simulations," *IEEE Transaction on Vehicular Technology*, vol. 62, no. 1, pp. 14–25, Jan. 2013.
24 A. Chandra, A. Prokeš, T. Mikulášek, J. Blumenstein, P. Kukolev, T. Zemen, and C. F. Mecklenbräuker, "Frequency-domain in-vehicle UWB channel modeling," *IEEE Transactions on Vehicular Technology*, vol. 65, no. 6, pp. 3929–3940, June 2016.
25 T. Kayser, J. V. Hagen, and W. Wiesbeck, " of antenna locations for wireless incar communication," in *URSI Int. Symp. Electromagnetic Theory*, Pisa, Italy, May 2004.
26 M. A. Peyrot-Solis, G. Galvan-Tejada, and H. Jardon-Aguilar, "State of the art in ultra-wideband antennas," in *2nd International Conference on Electrical and Electronics Engineering (ICEEE) and XI Conference on Electrical Engineering (CIE)*, Mexico City, Mexico, September 7-9 2005, pp. 101–105.
27 Z. shunshi, L. Xianling, and Y. Xiaorong, "UWB planar antenna technology," *Chinese Journal of Radio Science*, vol. 22, no. 2, pp. 308–315, April 2007.
28 W.-S. Lee, D.-Z. Kim, K.-J. Kim, and J.-W. Yu, "Wideband Planar Monopole Antennas With Dual Band-Notched Characteristics," *IEEE Transactions on Microwave Theory and Techniques*, vol. 54, no. 6, pp. 2800–2806, June 2006.
29 C. Yong, LuiWen-jun, C. Chong-hu, and C. Wei, "A compact frequency notched ultra-wideband antenna for multiple application," *Journal of Microwaves*, vol. 23, no. 1, pp. 20–24, Feb. 2007.
30 H. Deng, X. He, S. Liu, and Y. Xie, "A Novel Ultra Wideband Planar Antenna," in *Global Symposium on Millimeter Waves, GSMM*, 2008, pp. 288 – 290.
31 S. Adnan, R. A. Abd-Alhameed, S. Jones, H. I. Hraga, M. S. Bin-Melha, and E. A. Elkhazmi, "A modified printed monopole antenna for ULTRA-WIDEBAND applications," in *Proceedings of the Fourth European Conference on Antennas and Propagation (EuCAP)*, April 2010.
32 A. A. Kishk, X. H. Wu, and K. S. Ryu, "UWB Antenna for Wireless Communication and Detection Applications," in *IEEE International Conference on Ultra-Wideband (ICUWB)*, Sept. 2012, pp. 72–76.
33 I. J. Garcia Zuazola, J. C. Batchelor, J. M. H. Elmirghani, and N. J. Gomes, "UWB PIFA Antenna for simplified transceivers," *IET Electronics Letters*, vol. 46, no. 2, pp. 116–118, Jan. 2010.
34 H. Deng, J. Li, L. Yang, and T. Talty, "Intra-Vehicle UWB MIMO Channel Capacity," in *IEEE Wireless Communications and Networking Conference Workshops*, paris, April 2012, pp. 393–397.
35 A. Goldsmith, *Wireless Communications*. Cambridge University Press, NY, 2005.
36 M. Clark, M. Mulligan, and D. Jackson, "Fixed-Point Modeling in an Ultra Wideband Wireless Communication System," Matlab digest, May 2004.
37 C. A. Balanis, *Antenna Theory Analysis and Design*, 2nd ed. Wiley, 1997.
38 Y. Li, Y. Wang, and J. Lu, "Performance Analysis of Multi-User UWB Wireless Communication Systems," in *International Conference on Wireless VITAE*, Aalborg, Denmark, May 2009, pp. 152–155.
39 U. G. Schuster and H. Bolcskei, "Ultrawideband channel modeling on the basis of information-theoretic criteria," *IEEE Transactions on Wireless Communications*, vol. 6, no. 7, pp. 2464–2475, July 2007.
40 R. S. Elliott, "On discretizing continuous aperture distributions," *IEEE Transaction on Antennas and propagation*, vol. 25, no. 5, pp. 617–621, Sept. 1977.
41 N. T. Nguyen, A. V. Boriskin, A. Rolland, L. L. Coq, and R. Sauleau, "Shaped Lens-Like Dome for UWB Antennas With a Gaussian-Like Radiation Pattern," *IEEE Transaction on antennas and propagation*, vol. 61, no. 4, pp. 1658–1664, April 2013.